



Healing of simulated fault gouges aided by pressure solution: Results from rock analogue experiments

André Niemeijer,^{1,2,3} Chris Marone,^{2,3} and Derek Elsworth^{1,3}

Received 7 September 2007; revised 6 December 2007; accepted 15 January 2008; published 11 April 2008.

[1] Slide-hold-slide friction experiments are reported on fault gouges of salt and salt-muscovite mixtures to investigate the effects of fluids and phyllosilicates on strength gain. Healing rates of salt gouges in the presence of saturated brine are an order of magnitude higher than dry salt and water-saturated quartz at 65°C. Fault gouges consisting of salt-muscovite (80:20) mixtures show healing rates half that of 100 wt % salt; this is consistent with the effects of lower porosity and reduced dilation resulting from lower friction associated with muscovite. Half of the strength gain can be attributed to dilational work. The remainder of the strength gain can be explained by a microphysical model of compaction via pressure solution. Our model predicts the rate of contact area growth and of frictional restrengthening. The model predicts the observed rate of restrengthening for long hold periods for wet salt but underestimates the values for shorter hold periods. The short time response is attributed to strengthening of the grain boundary, elevating the resistance to frictional sliding on its interface, which is likely to be operative at longer hold periods as well but is masked by the strength gain owing to the increase in contact area. Our observations are consistent with an increased resistance to sliding of the contact at short term, the growth of the contact beyond this, and dilational hardening at all hold durations. To predict the magnitude and rates of healing in natural fault gouges under hydrothermal conditions, knowledge of the “state” of the fault gouge is required.

Citation: Niemeijer, A., C. Marone, and D. Elsworth (2008), Healing of simulated fault gouges aided by pressure solution: Results from rock analogue experiments, *J. Geophys. Res.*, 113, B04204, doi:10.1029/2007JB005376.

1. Introduction

[2] Fluids are important in the recovery of strength on faults between earthquakes [e.g., *Hickman et al.*, 1995]. They exert a strong influence on the behavior of the fault gouge through both mechanical and chemical effects [e.g., *Chester and Higgs*, 1992; *Kanagawa et al.*, 2000; *Kirby and Scholz*, 1984]. An increase in fluid pressure reduces the effective normal stress, effectively weakening the fault. Conversely, pressure solution compaction and/or mineral precipitation strengthen faults through an increase in packing density, an increase in contact area and/or an increase in the intrinsic strength (quality) of the sliding contacts. Despite its importance, little is known about the absolute rates of restrengthening (i.e., healing) under hydrothermal conditions. It is expected that the healing rate of a fault gouge will be strongly dependent on parameters such as the chemistry of the pore fluid, temperature and the “state” of

the fault gouge (e.g., the porosity, grain size distribution and the presence of shear bands). Moreover, it is known that phyllosilicates have a strong influence on the rates of pressure solution compaction and may act as inhibitors to contact strengthening [*Bos and Spiers*, 2000, 2001, 2002b; *Niemeijer and Spiers*, 2002, 2005, 2006]. However, much of the previous work has examined the response of pure quartz gouge at room temperature where pressure solution is minimally active or effectively absent. Moreover, previous studies have mostly neglected the possible effects of the “state” of the fault gouge; i.e., the absolute value of porosity, the grain size (distribution), and the possible effects of accumulated strain through evolution of the microstructure [*Niemeijer and Spiers*, 2007].

[3] Previous work on pure quartz gouges under hydrothermal conditions (up to 927°C) has shown that pressure solution has a significant effect on healing rates in simulated fault gouges [*Chester and Higgs*, 1992; *Fredrich and Evans*, 1992; *Karner et al.*, 1997; *Nakatani and Scholz*, 2004; *Tenthorey and Cox*, 2006; *Tenthorey et al.*, 2003; *Yasuhara et al.*, 2005]. There is a general consensus that the operation of pressure solution significantly enhances healing rates in experimental faults and fault gouges (with up to a ~0.1 increase in friction coefficient per decade increase in hold time; i.e., one order of magnitude higher than for dry or room temperature experiments) [*Marone*, 1998a, 1998b;

¹Department of Energy and Mineral Engineering, Pennsylvania State University, University Park, Pennsylvania, USA.

²Department of Geosciences, Pennsylvania State University, University Park, Pennsylvania, USA.

³G3 Center and Energy Institute, Pennsylvania State University, University Park, Pennsylvania, USA.

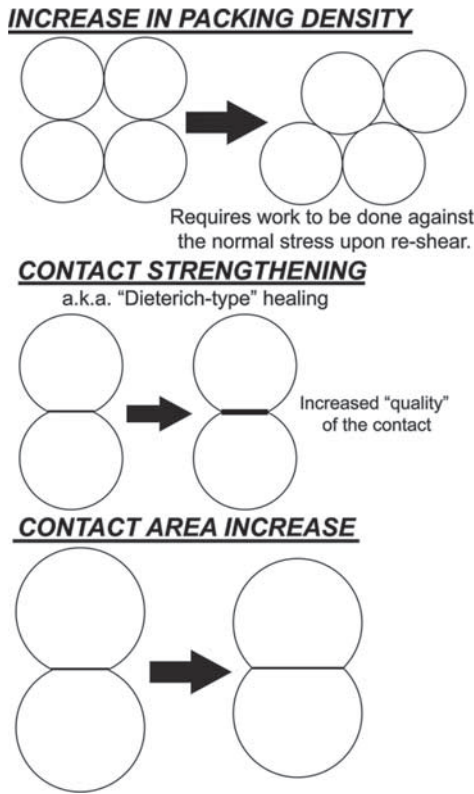


Figure 1. Cartoon illustrating possible mechanisms of restrengthening (Dieterich-type healing) [e.g., *Marone, 1998a; Scholz, 2002*].

Scholz, 2002]. Unfortunately, none of these studies has explicitly investigated the individual competing mechanisms through which pressure solution may strengthen gouges. Restrengthening may result from (1) lithification [*Karner et al., 1997*]; (2) replacement of adhesive contacts with welded contacts by mineral precipitation and cementation, increasing the cohesion of the fault [*Fredrich and Evans, 1992; Tenthorey and Cox, 2006; Tenthorey et al., 2003*]; or (3) compaction and increased grain-to-grain contact area [*Nakatani and Scholz, 2004; Yasuhara et al., 2005*]. It is likely that restrengthening under hydrothermal conditions is a combination of the three, with each of the mechanisms being important under different conditions. The presence or absence of phyllosilicates will have the most influence in the regime where strengthening is dominated by welding of sliding contacts, whereas grain size and porosity will play a central role in restrengthening through lithification (porosity reduction, requiring work against the normal stress) and contact area growth, because pressure solution rates are related to porosity and inversely related to grain size [e.g., *Spiers et al., 2004*].

[4] In this study, we report slide-hold-slide experiments on simulated fault gouges consisting of salt and salt-muscovite mixtures under room temperature conditions to investigate the effects of the “state” of the fault gouge, the presence or absence of phyllosilicates, and the presence or absence of a reactive pore fluid on healing rates.

[5] Following *Lehner [1995], Bos and Spiers [2000, 2002a]* and *Niemeijer and Spiers [2006, 2007]* the combined energy and entropy balance for a representative unit volume of fault rock during deformation can be written

$$\tau\dot{\gamma} + \sigma_n\dot{\epsilon} = \dot{f} + \dot{\Delta} + \dot{A}_{gb}\gamma_{gb} + \dot{A}_{sl}\gamma_{sl}, \quad (1)$$

where a closed system is assumed with respect to solid mass. In this equation, τ is the shear stress acting on the fault rock, $\dot{\gamma}$ is the shear strain rate, σ_n is the effective normal stress on the fault (compression positive), and $\dot{\epsilon}$ is the compactional strain rate (compaction positive). The summed product of these stress and strain rates is equated to dissipative processes where \dot{f} is the rate of change of Helmholtz free energy of the solid phase per unit volume, $\dot{\Delta}$ is the volumetric energy dissipation rate by all irreversible processes, \dot{A}_{gb} is the rate of change in grain boundary surface area per unit volume, γ_{gb} is the grain boundary surface energy, \dot{A}_{sl} is the rate of change of solid-liquid interfacial area per unit volume and γ_{sl} is the solid-liquid interfacial energy. The right-hand side of (1) represents the sum of the energy dissipation rates of all microscale processes operating per unit volume (Δ), plus changes in the Helmholtz free energy stored in the solid part of the system, plus changes in surface energy caused by changes in grain boundary and pore wall area. Dividing now by $\dot{\gamma}$ [*Bos and Spiers, 2000, 2002a; Niemeijer and Spiers, 2006*], the measured shear stress or shear strength can be written

$$\tau = \tau_x - \frac{d\epsilon_v}{d\gamma} \cdot \sigma_n, \quad (2)$$

where $d\epsilon_v/d\gamma$ represents an instantaneous dilation rate and is related to the dilation angle by $\tan(\psi) = d\epsilon_v/d\gamma$ analogous to that familiar in soil mechanics [e.g., *Paterson, 1995*], and where

$$\tau_x = \frac{df}{d\gamma} + \frac{d\Delta}{d\gamma} + \frac{dA_{gb}}{d\gamma} \gamma_{gb} + \frac{dA_{sl}}{d\gamma} \gamma_{sl}. \quad (3)$$

The quantity τ_x represents the contribution to shear strength of all energy dissipation and storage processes operating in the gouge. Ignoring minor changes in Helmholtz free energy, it is evident from (2) and (3) that strengthening of a deforming granular fault gouge may occur for three basic reasons (summarized in Figure 1).

[6] First, gouge compaction may increase the packing density so that upon reshearing the gouge needs to dilate, requiring work against the normal stress ($-d\epsilon/d\gamma$). Second, the gouge may restrengthen through an increase in contact bonding between particles in the gouge. The increased bonding may increase the grain boundary friction coefficient and/or the grain boundary cohesion. This then increases the average contact sliding strength and thereby the total frictional dissipation ($d\Delta/d\gamma$) owing to intergranular slip. Third, the gouge may strengthen by an increase in grain contact area (relative to pore wall area). Contact area growth may increase shear strength via an increase in friction and/or through increased cohesive strength, whereas it reduces the local normal stress, lowering pressure solution

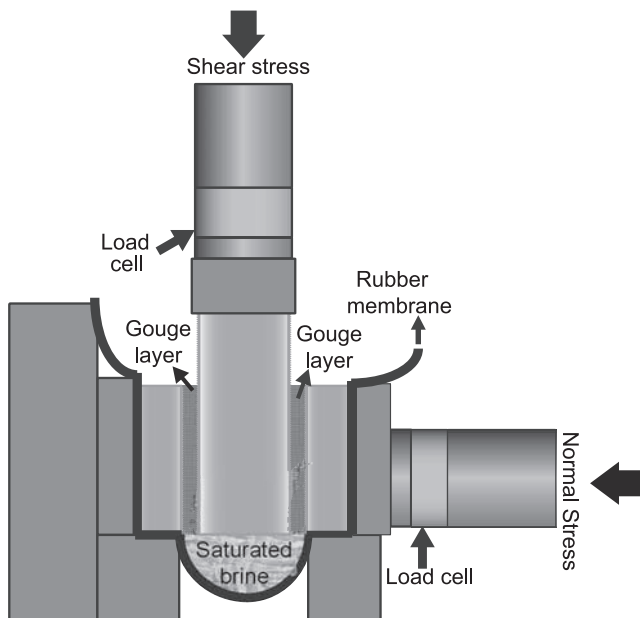


Figure 2. Schematic diagram illustrating the experimental setup.

rates. In general, fault gouge healing will be a combination of the three. However, the amount of restrengthening owing to an increase in packing density can be derived from experimental data by measuring volume changes during reshearing. Using these volume changes, the measured shear stress can be recast in terms of τ_x or μ_x :

$$\mu_x = \frac{\tau_{\text{measured}}}{\sigma_n} - \frac{d\varepsilon}{d\gamma} \quad (4)$$

In this way the amount of restrengthening by purely dilational work against the normal stress can be evaluated. With this dilational influence removed, the role of the other processes (contact growth and “quality” of grain-grain contacts) may be evaluated. This is the focus of our study.

2. Experimental Methods

[7] A series of slide-hold-slide experiments was performed on simulated fault gouges consisting of granular salt and mixtures of granular salt and muscovite. The granular salt was derived from natural rock salt, crushed then sieved to retain a grain size fraction of 106–212 μm . The initial grain size distribution was determined using a Malvern particle size analyzer and the mean grain size was 159 μm . A commercially available muscovite (Internatio B. V., Netherlands) with an average grain size of 13 μm was used as received. In each experiment, two identical gouge layers were built with an initial layer thickness of ~ 5 mm. The exact thickness and mass of each layer was recorded. The sample assembly consists of a central block sandwiched between two side blocks. The surfaces that contact the gouge layers are grooved perpendicular to the sliding direction; groove height and spacing is 0.5 mm and 1 mm, respectively. The assembled sample was placed in the

biaxial loading frame surrounded by a rubber membrane in which the pore fluid (saturated brine) was poured. The sample was then left to saturate for 45 min after which an initial normal load of 10 MPa was applied. One dry experiment was performed inside a plastic bag containing anhydrous CaSO_4 and a humidity sensor. The humidity was monitored throughout the experiment and never exceeded 6%.

[8] After initial loading, the center block was driven down (Figure 2) at a displacement rate of 5 $\mu\text{m/s}$, causing shear of the layers through a displacement of 10 mm; the normal stress was then reduced to 5 MPa and the slide-hold-slide tests were initiated. This run-in phase was used to minimize the effects of grain size reduction by cataclasis during the slide-hold-slide tests. The displacement rate during “slide” periods was 5 $\mu\text{m/s}$ for a displacement of 2.5 mm. Hold periods were 30, 100, 300, 1000, 3000 and 10,000 s. We also performed two experiments with the same hold periods, but in a “reverse” mode; i.e., the longest hold period first. During the entire experiment, the porosity of the sample was recorded by the displacement of the horizontal piston. When the experiment was finished, the sample assembly was removed from the loading frame and flushed with iso-butanol to remove any remaining pore fluid, and the gouge material was carefully removed and dried at 65°C for 24 hours before epoxy impregnation and thin section cutting.

3. Results

[9] In all our experiments, the recorded variables are instantaneous dilation rate and the evolution of shear stress (force) with displacement. These observations provide changes in porosity and shear stress as a function of hold periods, degree of chemical activity via fluid saturation or humidity and the presence or absence of phyllosilicates and are used to examine the mechanisms of strength recovery.

3.1. Mechanical Response

[10] In Figure 3, we show a typical plot of the evolution of the apparent friction coefficient (shear stress divided by normal stress) and porosity as a function of shear displacement (corrected for the elastic stiffness of the loading frame) for the entire experiment. The porosity was determined by measuring the displacement of the horizontal piston and correcting for layer thinning owing to the geometry of the experimental setup [Scott *et al.*, 1994]. In all tests, the friction coefficient initially increases until a yield point, after which the strength drops and then increases steadily for the room-dry and brine-saturated salt samples during the run-in phase. In contrast, friction drops for the nominally dry salt sample and for layers containing 20 wt % muscovite.

[11] Upon reloading of the samples after the reduction in normal stress to 5 MPa, the friction coefficient shows a sharp peak followed by gradual weakening (samples without muscovite) or sliding at a constant friction level (samples with muscovite). Porosity decreases for all samples during the initial run-in of 10 mm displacement, but reaches a more or less steady state at the end of the run-in phase. Upon reloading of the samples after the reduction in normal stress, all samples showed dilation, which was highest for the brine-saturated salt samples (p1384 and p1414). After

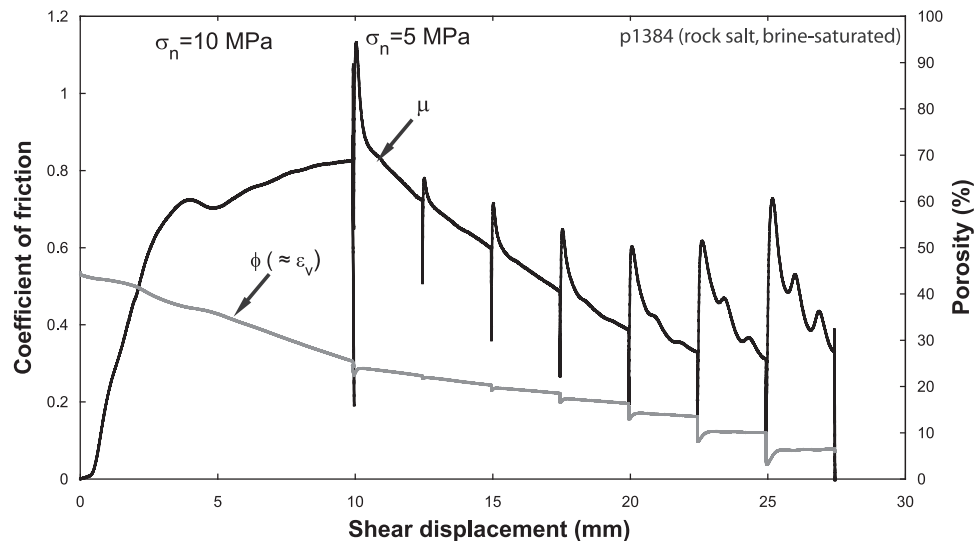


Figure 3. Plot showing friction coefficient and porosity versus shear displacement for sample p1384 (rock salt, brine-saturated). Porosity is equivalent to the volumetric strain ($= (\phi_0 - \phi)/\phi_0$).

the initial dilation, all samples with fluid showed continuous compaction, in contrast to the “dry” samples which showed continuous dilation (with exception of the hold periods). The total compaction was highest for the brine-saturated samples deformed in the “forward” mode (short to long hold periods) containing 20 wt % muscovite (porosity reduced to $\sim 3.7\%$, see also Table 1), whereas the dry experiment (p1413, less than 6% humidity) had a final porosity of 22%, owing to ongoing dilatation during the slide-hold-slide phase (at a normal stress of 5 MPa) of the experiment.

[12] Figure 4 shows selected curves of friction coefficient and porosity vs shear displacement for the slide-hold-slide phase of the experiments. All samples show an initial sharp increase in friction coefficient to a well-defined peak stress. After this, all 100 wt % salt samples showed continuous weakening, with the experiments performed under dry conditions developing stick-slip instabilities after a displacement of ~ 5 mm. The muscovite-salt mixture, however, showed no significant weakening over the displacement investigated. Upon reshear, a sharp increase in friction coefficient is observed accompanied by dilation, followed by gradual weakening, except for the salt-muscovite mixtures, which reach a steady state value after ~ 1 mm of reshear.

[13] In Figure 5, we show the relaxation of shear stress in terms of the change in friction coefficient and the change in porosity for selected samples and hold periods of 100 and

10,000 s. The scales have been kept the same for ready comparison. In all brine-saturated samples, the friction coefficient drops rapidly during all hold periods, whereas the nominally dry experiment (p1413, $< 6\%$ humidity) shows virtually no change in friction coefficient. The rate of change in friction coefficient is larger for short hold periods in samples deformed in the “forward” mode (i.e., longest hold period last; see Figures 5b and 5c) and smaller for short hold periods in samples deformed in the “reverse” mode (i.e., longest hold period first; see Figures 5d and 5e). Porosity drops rapidly during hold periods for all brine-saturated samples and the rate of porosity change is similar for all hold periods. The total change of porosity increases with increasing hold duration and is the highest for the 100 wt % salt samples.

3.2. Microstructures

[14] We show representative microstructures of three deformed samples in Figures 6 and 7. In Figure 6a, the microstructure is shown of sample p1413 deformed under nominally dry conditions ($< 6\%$ humidity). The gouge appears highly porous with no evident signs of localization, although argument could be made for some regions with a somewhat higher porosity in a Riedel shear orientation (angle of $20\text{--}30^\circ$ to the shear zone boundary). Grains appear blocky and the grain size is reduced with respect to the initial median grain size. Image analysis yields a median grain size of $48 \mu\text{m}$, but the standard deviation is quite large ($42 \mu\text{m}$).

Table 1. List of Experiments Performed and Corresponding Experimental Conditions

Sample ID	Composition, wt %		Normal Stress, MPa	Velocity, $\mu\text{m/s}$	SHS Periods, s	Total Shear Strain	Final Porosity, %
	Salt/Muscovite	Pore Fluid					
p1383	100/0	room-dry	10–5	5	30–100–300–1,000–3,000–10,000	11.37	21.0
p1384	100/0	saturated brine	10–5	5	30–100–300–1,000–3,000–10,000	11.51	6.6
p1385	80/20	saturated brine	10–5	5	30–100–300–1,000–3,000–10,000	12.71	3.7
p1413	100/0	humidity $< 6\%$	10–5	5	30–100–300–1,000–3,000–10,000	10.25	18.2
p1414	80/20	saturated brine	10–5	5	10,000–3,000–1,000–300–100–30	11.66	14.7
p1415	80/20	saturated brine	10–5	5	10,000–3,000–1,000–300–100–30	12.38	14.2

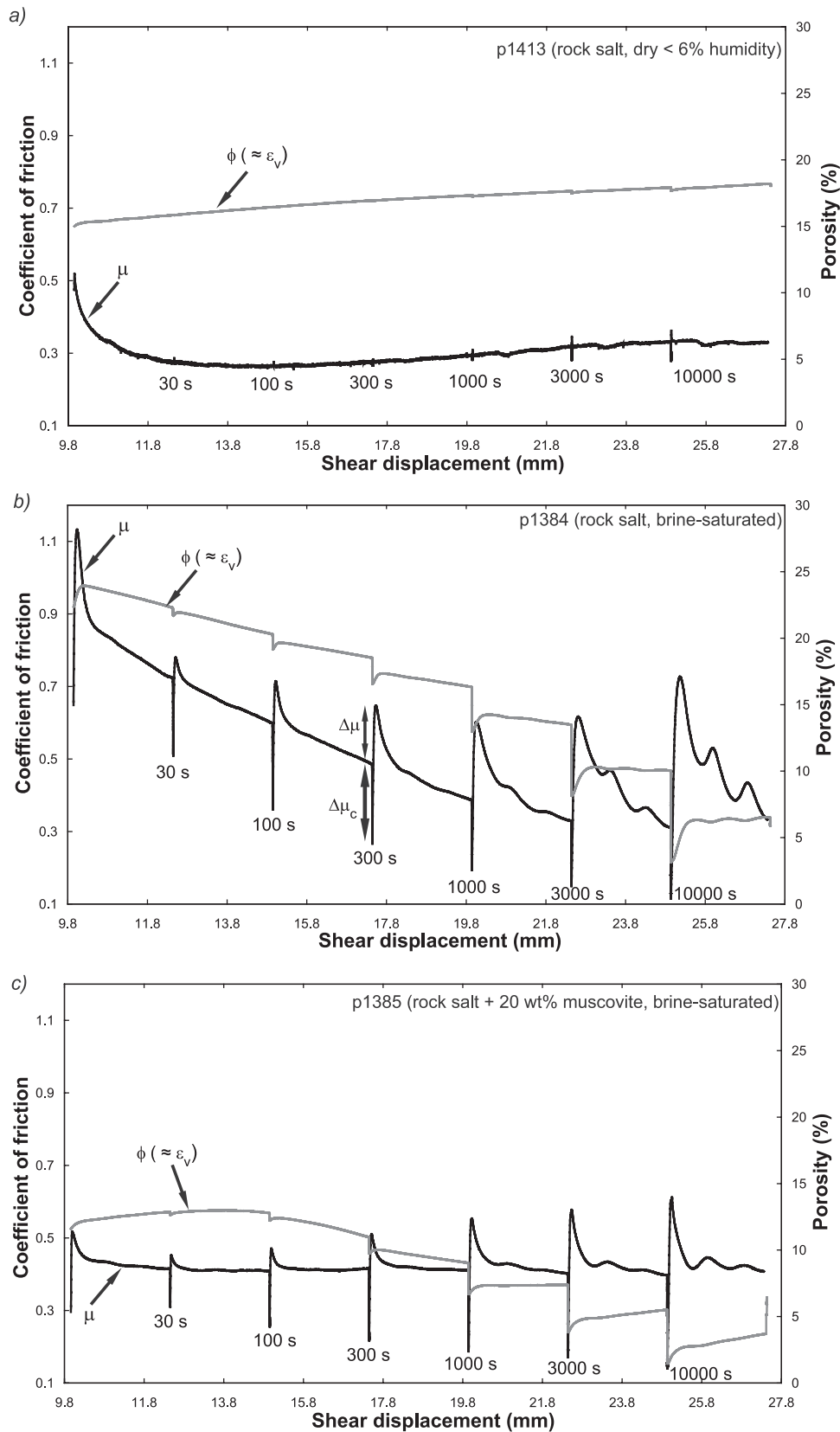


Figure 4. Friction coefficient and porosity versus shear displacement during the slide-hold-slide part of the experiments. Normal stress is 5 MPa in all cases. $\Delta\mu$ is defined as the peak friction coefficient divided by the steady state friction coefficient, and $\Delta\mu_c$ is the change in friction coefficient during a hold period: (a) p1413 (rock salt dry < 6% humidity), (b) p1384 (rock salt, brine-saturated), and (c) p1385 (rock salt + 20 wt % muscovite, brine-saturated).

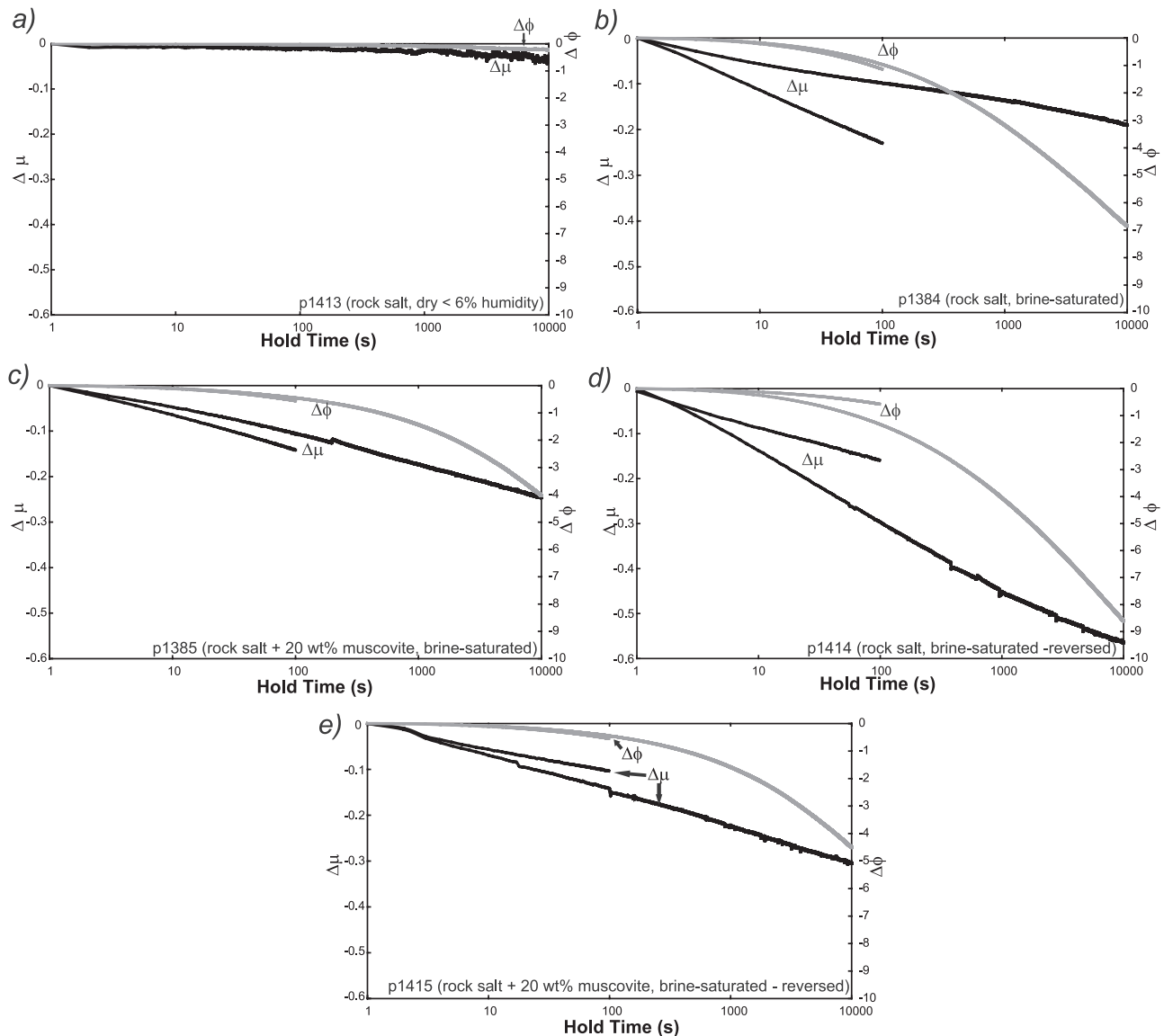


Figure 5. Plot showing the evolution of friction coefficient (black lines) and porosity (gray lines) during hold periods of 100 and 10000 s: (a) p1413 (rock salt dry < 6% humidity), (b) p1384 (rock salt, brine-saturated), (c) p1385 (rock salt + 20 wt % muscovite, brine-saturated), (d) p1414 (rock salt, brine-saturated, reversed), and (e) p1415 (rock salt + 20 wt % muscovite, brine-saturated, reversed).

[15] Sample p1384 (brine-saturated, 100 wt % salt) shows a lower overall porosity than the dry sample, but porosity is still evident (Figures 6b and 7a). Grain size analysis was difficult on this sample, because grain boundaries were hardly discernible under SEM-BSE, presumably because of agglomeration of the grains by compaction. This agglomeration also leads to a heterogeneous distribution of the porosity. On closer inspection, many agglomerates can be shown to consist of several individual grains with long, tight grain contacts (Figure 7a). The grains appear more equant than in the dry case and slightly elongated with respect to the direction of shear. Grain-to-grain indentation, indicative of pressure solution, is ubiquitous (Figure 7a). The gouge consisting of salt-muscovite (p1385, Figures 6c and 7b) shows the lowest porosity of all samples, but dilatant zones are obvious. These are presumably formed during the unloading of the samples and their orientation (angles of

25°–30° and 50°–60° to the shear zone boundary) suggests that they are former Riedel R1 and R2 shear bands. None of the dilatant zones seems to be throughgoing and some flatten to an angle almost parallel to the shear zone boundary. Also, the dilatant zones appear to anastomose, changing orientation when followed along the gouge. The muscovite grains wrap around most of the salt grains and we estimate 80% of the contacts consist of salt-muscovite. The grain contacts without muscovite appear tight (Figure 7b), in contrast to muscovite-bearing contacts that appear fairly open. Again, numerous grain-to-grain indentations can be found throughout the gouge.

4. Discussion

[16] Independently varied in successive experiments were porosity via the degree of compaction, the duration and the

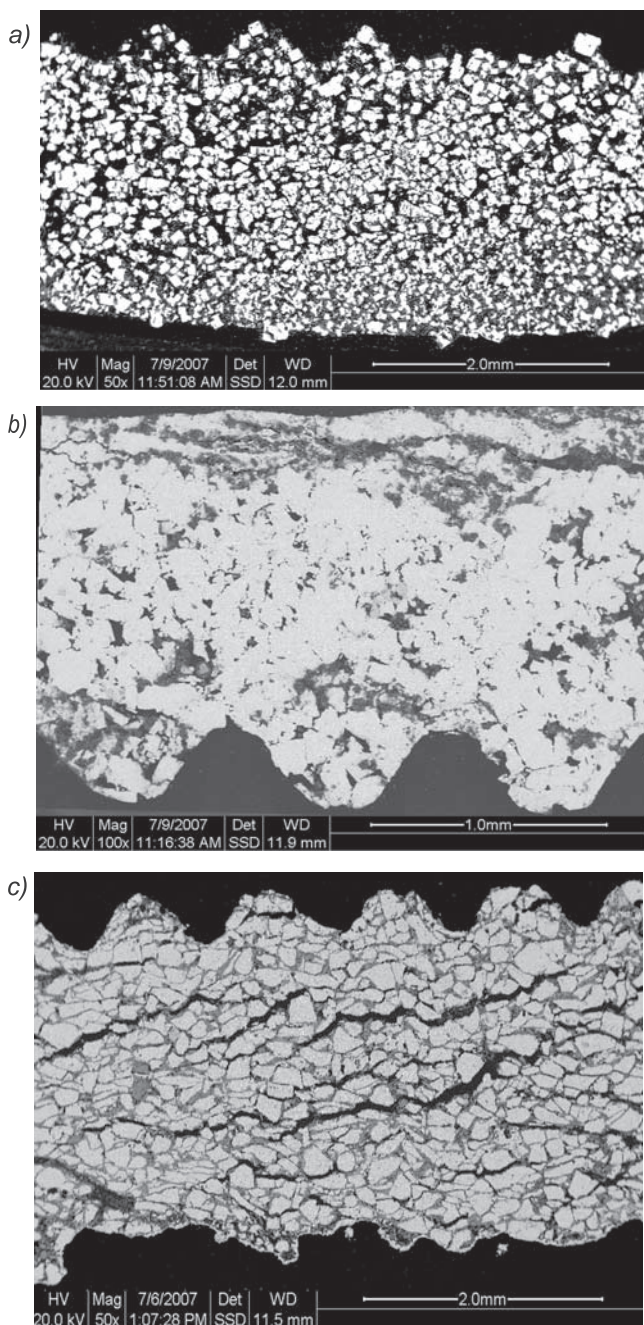


Figure 6. SEM BSE images of the final gouge microstructure. Shear sense is sinistral: (a) p1413 (rock salt dry < 6% humidity), (b) p1384 (rock salt, brine-saturated), and (c) p1385 (rock salt + 20 wt % muscovite, brine-saturated).

order of applying hold periods, the presence or absence of phyllosilicates, and degree of saturation or humidity within the sample. Although the influence of dilation, and the quality and quantity of the contact growth jointly affect strength gain and loss, these parametric separations are used to distinguish their relative influence. Principal influences on strength are expected to be porosity via dilation, hold length and saturation *via* the quantity (area) of contacts, and the sequencing of hold *via* the quality of the contact. This is the premise of the experimental suite, discussed below.

4.1. Dilation

[17] In Figures 8 and 9, we show selected curves of the evolution of friction coefficient along with the dilation-corrected apparent friction coefficient (μ_x , see equation (4)) and instantaneous dilation rate as a function of shear displacement after hold periods of 100 and 10,000 s, respectively. From these, we observe that the peak in dilation rate always precedes the peak in friction coefficient. Moreover, all curves of μ_x exhibit a peak, which means that dilational work against the normal stress alone cannot explain the observed healing. However, there is a distinct difference between the curves of μ and μ_x , confirming a contribution from dilation to the observed strengthening. This effect is most clear from the evolution of healing rates (i.e., $\Delta\mu/\Delta t$ and $\Delta\mu_x/\Delta t$) with hold time, as shown in

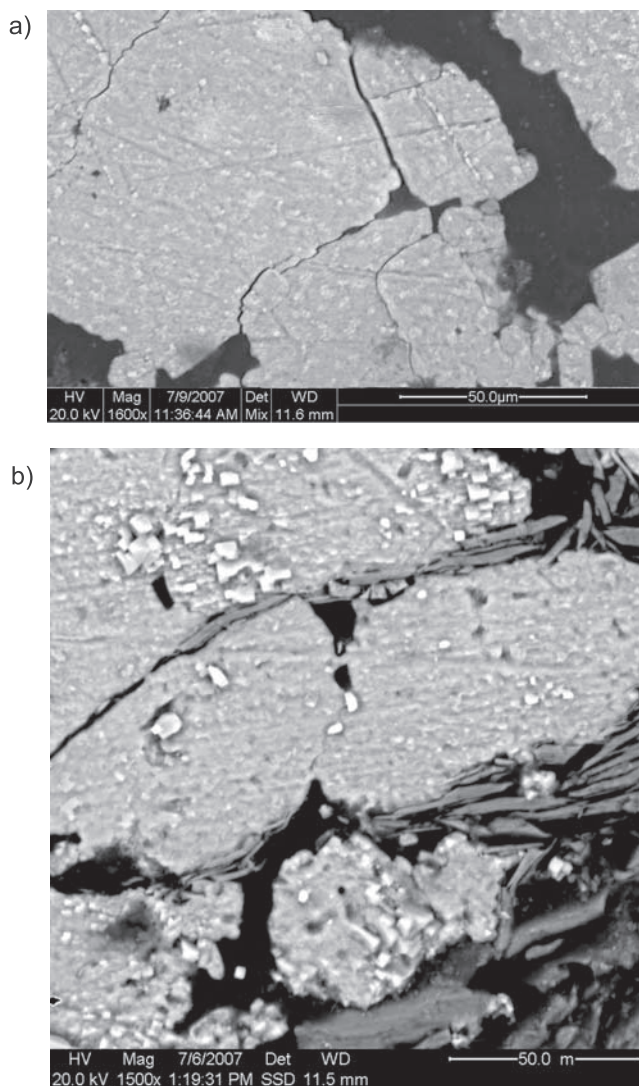


Figure 7. SEM BSE of the final gouge microstructure. Shear sense is sinistral: (a) p1384 (rock salt, brine-saturated) showing grain-to-grain indentations, indicative for the operation of pressure solution and (b) p1385 (rock salt + 20 wt % muscovite, brine-saturated) showing the presence of muscovite in most grain contacts. Contacts without muscovite appear highly cemented.

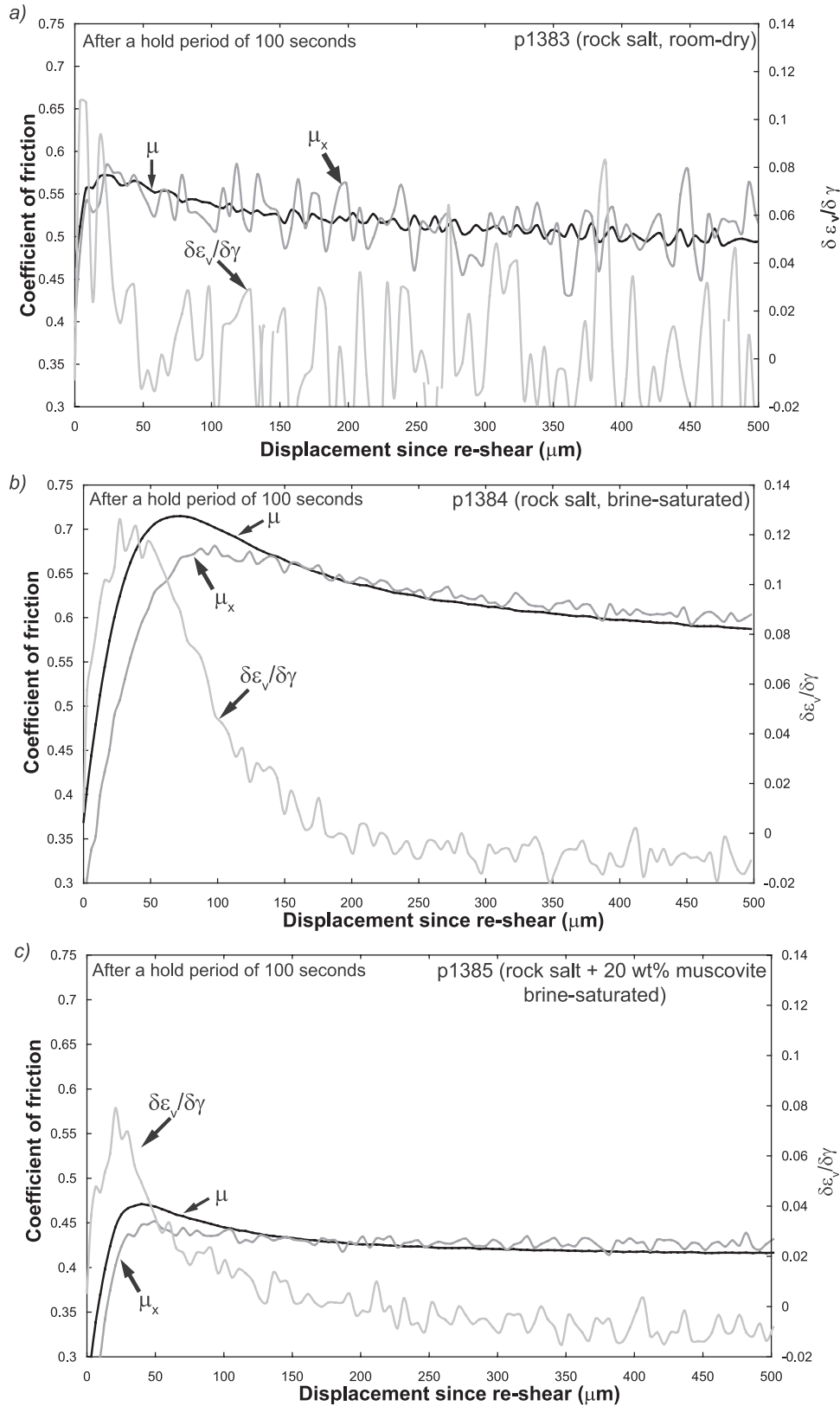


Figure 8. Plot showing the evolution of friction coefficient, corrected friction coefficient and dilatation upon reshear after a hold period of 100 s: (a) p1413 (rock salt dry < 6% humidity), (b) p1384 (rock salt, brine-saturated), and (c) p1385 (rock salt + 20 wt % muscovite, brine-saturated).

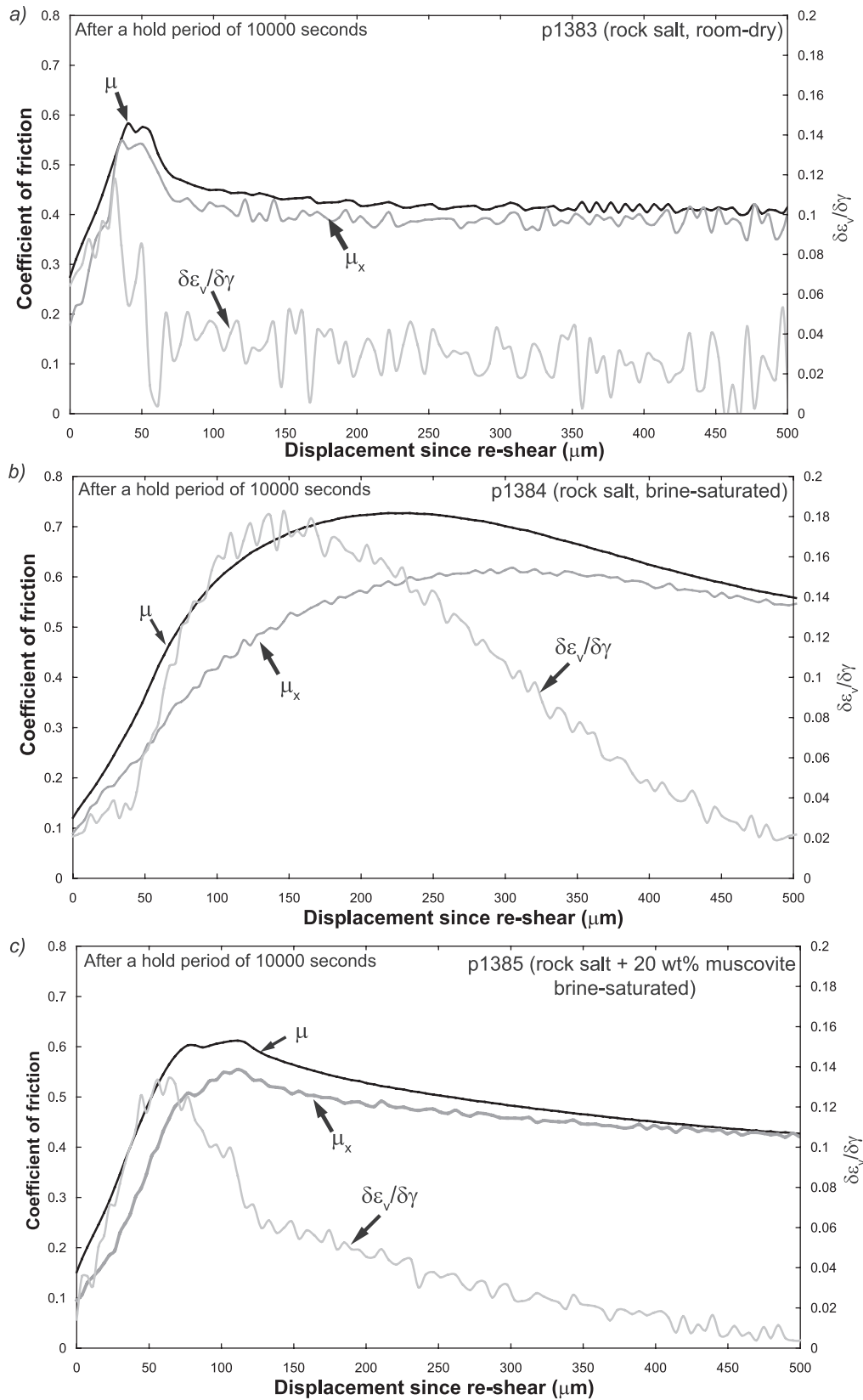


Figure 9. Plot showing the evolution of friction coefficient, corrected friction coefficient and dilatation upon reshear after a hold period of 10,000 s: (a) p1413 (rock salt dry < 6% humidity), (b) p1384 (rock salt, brine-saturated), and (c) p1385 (rock salt + 20 wt % muscovite, brine-saturated).

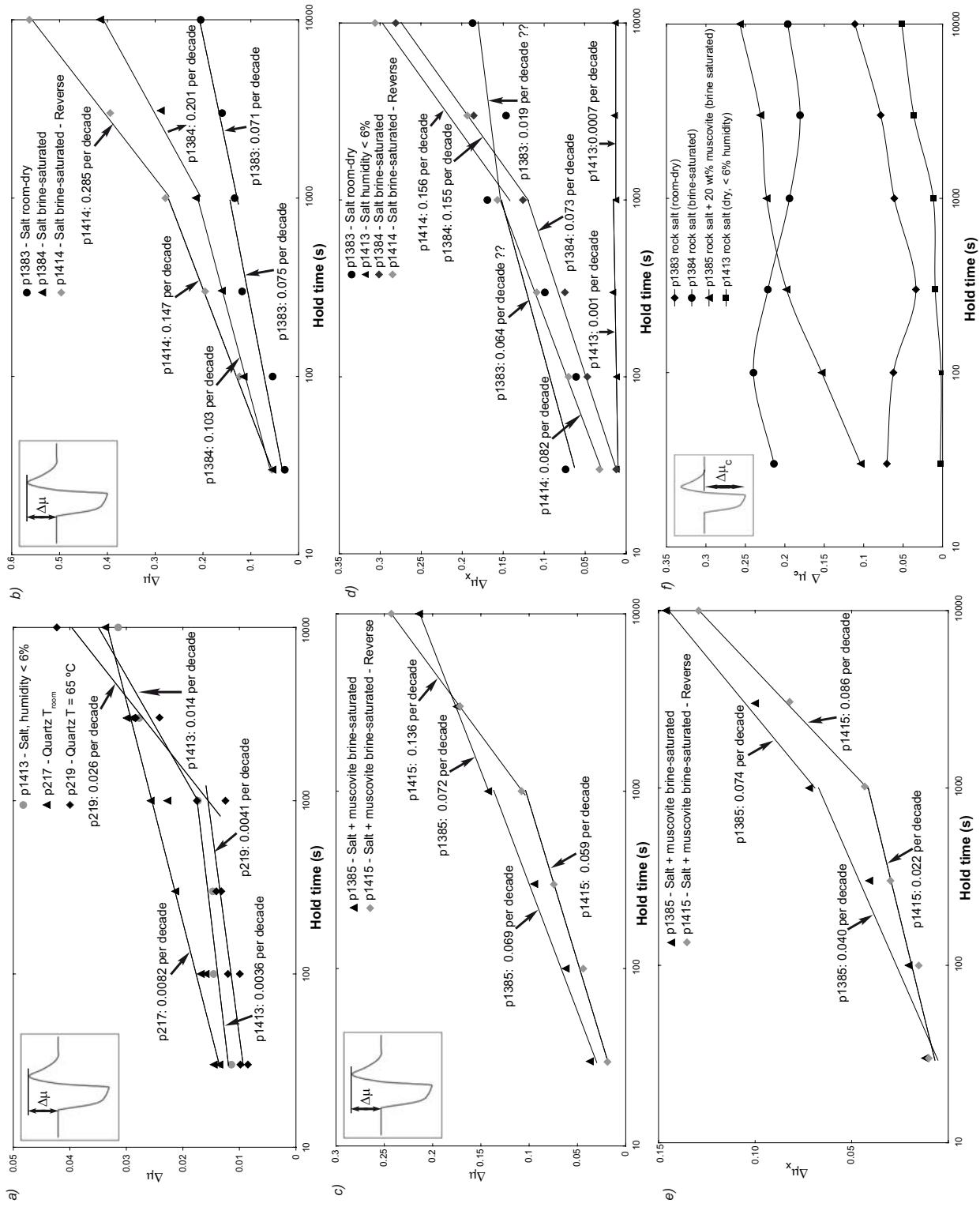


Figure 10

Figure 10. Here, we show changes in apparent friction coefficient as a function of hold time, following the definitions of *Yasuhara et al.* [2005] and including the change in μ_x (equation (4)). For comparison, we also show the data of experiments p217 and p219 from *Yasuhara et al.* [2005]. Our experiments on granular salt show greater healing than observed in quartz under low-temperature conditions, as evidenced by the slope of the log linear trend in $\Delta\mu$. Healing rates as high as 0.285 per decade were observed for the 100 wt % salt sample in the presence of saturated brine. All data can be fit by a log linear trend, but fit more closely a bilinear trend [*Yasuhara et al.*, 2005] with a break in slope occurring between 300 and 1000 s.

[18] As mentioned earlier the fault gouge may restrengthen for three basic reasons. We can evaluate the effect of dilational work by comparing $\Delta\mu_x$ with $\Delta\mu$. If all the increase in shear strength was due to an increase in grain packing requiring dilational work against the normal stress during reloading after hold periods (as suggested by *Yasuhara et al.* [2005] for the short hold periods), $\Delta\mu_x$ would be zero. We show $\Delta\mu_x$ in Figure 10 for all our experiments and representative plots of the evolution of μ_x as a function of displacement in Figures 8 and 9. From all these plots, it is clear that dilational work alone cannot explain the observed changes in shear strength of the gouge, but does account for up to 80% of the increase in strength for shorter hold periods. The relative contribution of dilational work decreases with increasing strain and increasing hold period. No significant difference is observed between the 100 wt % salt samples and salt-muscovite mixtures. We will focus on the $\Delta\mu_x$ data in our discussion from now on, since this parameter does not contain the dilational effect and thus better describes the intrinsic strengthening of the gouge.

4.2. Quality Versus Total Area of Grain Contacts

[19] Our healing data show a break in slope at hold periods between 300 and 1000 s. Previous studies on quartz under conditions where pressure solution might be active have also observed a break in slope at similar hold periods [*Frye and Marone*, 2002; *Nakatani and Scholz*, 2004; *Yasuhara et al.*, 2005]. The break in slope suggests that around hold times of 300 to 1000 s, there is a switch in the dominant strengthening mechanism. We propose that this switch is the activation of pressure solution compaction, which causes an additional strengthening by an increase in average grain-to-grain contacts area of the fault gouge. Then, the initial strengthening at short hold periods is thought to be a “Dieterich-type” healing, where the asperities at contacts restrengthen via a solution-aided mechanism (see also Figure 1). This short-term restrengthening probably is also active at longer hold periods but is interpreted to be overwhelmed by the strengthening owing to an increase in contact area. The longer-term strengthening cannot occur at short hold periods, because the time is too short for pressure solution to increase the contact area

by a substantial amount. The cutoff time, t_c , for pressure solution aided strengthening can be calculated from

$$t_c = L^2/D, \quad (5)$$

where D is the diffusion coefficient for transport of dissolved matter in the grain boundary fluid and L is the characteristic path length of diffusion, which is proportional to grain size and contact junction dimension. Equation (5) assumes that diffusion is the rate-limiting process in pressure solution compaction, which is the case for salt at room temperature, but might not be the case for quartz [e.g., *Niemeijer et al.*, 2002]. Taking the diffusion coefficient to be 10^{-11} m²/s [e.g., *Spiers et al.*, 2004] and the initial median grain size as the length of the grain contact, we calculate a cutoff time of ~ 1500 s. This is a maximum estimate for the cutoff time, since we used our initial grain size as a maximum estimate for the length of the grain contact. Using a more realistic diffusional path length of 50 μm would yield a cutoff time of 250 s. If we consider the length scale of asperities on the contact from an island-channel structures [e.g., *Dysthe et al.*, 2002; *Schutjens and Spiers*, 1999], the cutoff time is reduced even further. Considering the uncertainty both in diffusion coefficient and the actual diffusion path length, this calculation suggests that pressure solution is a feasible contributor to the observed behavior.

4.3. Increase of Contact Area

[20] From our previous discussion, it is apparent that there could be three strengthening mechanisms that operate at long timescales (>300 s). In this section we focus on what appears to be the dominant strengthening mechanism at long hold periods. We assume that any short-term Dieterich-type strengthening is swamped by the long-term strengthening, and also that the effects of dilational work have already been removed from the observed response (i.e., we consider changes in $\Delta\mu_x$ alone). From our microstructural observations and mechanical data, we conclude that pressure solution is the dominant deformation mechanism during hold periods. Microstructural observations suggest strengthening of the fault gouges occurs via an increase in contact area by compaction via pressure solution for hold periods longer than 300 s. The restrengthening is thus a strong function of the rate of pressure solution compaction, which depends on porosity, grain size, presence or absence of a phyllosilicate phase and chemistry of the pore fluid. In the case of our experiments, the porosity dependence is evident from the comparison of the healing and relaxation rates (i.e., the change of apparent friction coefficient during a hold period, $\Delta\mu_c/\Delta t$) of the forward and reverse experiments. The reverse experiments show higher healing rates than the forward experiments, since the average rate of pressure solution compaction is larger in the longer hold periods owing to the higher porosity of the gouge at the start

Figure 10. (a–c) Change in the friction coefficient as a function of hold time. Values for log linear fits through the data points are shown. (d and e) Change in the friction coefficient corrected for dilational work against the normal stress. Values for log linear fits through the data points are shown. (f) Total reduction of apparent friction coefficient during hold periods as a function of hold period.

of the hold. Moreover, the rate of change of apparent friction coefficient is highest for short periods (low strain/high porosity) in the case of the forward experiments and for long periods (low strain/high porosity) in the case of the reverse experiments (compare Figures 5b and 5c with Figures 5d and 5e). This can be explained by the smaller contact area in gouges with high porosity accommodating the shear stress. Dissipation of these stresses is faster for the smaller contact areas. Further evidence for this mechanistic model can be found in the observation that the total amount of change in apparent friction coefficient does not change with an increase in hold period for the 100 wt % salt samples (Figure 10f). This can be explained by the progressive decrease in porosity and related increase in contact area with increasing strain. The increasing contact area leads to a decrease in relaxation rate, thereby lowering the total amount of stress relaxed over time.

[21] However, experimental evidence and microstructural observations suggest that compaction via pressure solution in aggregates containing a phyllosilicate phase is faster [Bjørkum, 1996; Gundersen *et al.*, 2002; Heald, 1959; Renard *et al.*, 2001], which implies that our salt-muscovite gouges should strengthen more. There are two observations to explain this apparent discrepancy. First, the salt-muscovite gouges retain a lower porosity during sliding than the 100 wt % salt gouges, probably owing to the presence of easy sliding surfaces provided by the muscovite grains requiring less dilatation. If the porosity of a gouge is lower at the time of halting of the sliding, compaction rates will be lower and thus the increase in contact area for a given time period will be lower. Secondly, the presence of muscovite grains between salt grains hinders strengthening of the contact. Salt-salt contacts presumably have a higher strength than salt-muscovite contacts and will be more prone to strengthening. Similar conclusions were reached in an earlier experimental study on salt-muscovite gouge in a ring shear apparatus by Niemeijer and Spiers [2006]. They observed healing rates that depend on the sliding velocity and which are similar to the healing rates we observed.

5. Microphysical Model

[22] We develop a quantitative microphysical model by starting from the procedure of Yasuhara *et al.* [2005], with the distinction that we compare the model output to values of $\Delta\mu_x$ from only long hold periods. In this way, we separate out the effects of dilational work and contact strengthening and isolate the effect of pressure solution compaction on strengthening of fault gouges.

5.1. Analysis

[23] The model assumes a geometry of uniform spheres in a simple cubic packing arrangement [e.g., Dewers and Ortoleva, 1990; Gundersen *et al.*, 2002; He *et al.*, 2002; Lehner, 1995; Niemeijer *et al.*, 2002; Paterson, 1995; Renard *et al.*, 1997, 1999; Spiers *et al.*, 1990, 2004]. Using this geometry, the porosity and contact area for the aggregate can be computed at any given time. Furthermore, we will use the porosities at the start of each sliding period as the starting porosity in our model and we will assume a closed system.

[24] Now, compaction via pressure solution is driven by a gradient in chemical potential between the grain boundary and the pore, given by

$$\Delta\Psi_n = (\sigma_n - p_f) \cdot \Omega_s, \quad (6)$$

where $\Delta\psi_n$ is the gradient in chemical potential, σ_n is the local normal stress, p_f is the fluid pressure and Ω_s is the molar volume of the solid and we neglect any changes in Helmholtz free energy. This gradient in chemical potential drives the three serial processes of dissolution at the grain boundary, diffusion of dissolved matter along the grain boundary and precipitation of matter in the pore space. The compaction rate will be governed by the slowest of these three processes and since it is well established that for salt at room temperature the rate limiting process is diffusion, we will focus on diffusion only. The diffusive flux of material is governed by Fick's law and is given by

$$J = \rho_f \cdot D_{gb} \cdot \nabla C, \quad (7)$$

where J is the mass flux, ρ_f is fluid density, D_{gb} is the grain boundary diffusion coefficient and ∇C is the concentration gradient along the grain boundary. At each grain contact, the flux acts through a diffusion window of size $w \cdot \delta$, where w is the width of the contact and δ is the thickness of the grain boundary fluid. The rate of mass transfer per contact (in kg/s) is then

$$J^* = w \cdot \delta \cdot \rho_f \cdot D_{gb} \cdot \nabla C. \quad (8)$$

Now, using the standard relation between the chemical potential of dissolved solid and its concentration, we write the difference in chemical potential between grain boundary and pore space as

$$\Delta\Psi = RT \ln \frac{C_s + \Delta C}{C_s} \approx RT \frac{\Delta C}{C_0}. \quad (9)$$

After integration of equation (8) from the center of the contact to the edge of the contact, equations (9) and (6) can be substituted and after division by the solid density, gives the total mass flux in m^3/s out of the grain boundary:

$$J = \frac{\rho_f D_{gb} \delta C_0 \sigma_n \Omega_s}{\rho_s RT}. \quad (10)$$

Averaging the mass flux over the contact area, yields the convergence velocity of the contact in m/s. In the model, the initial porosity yields an initial contact area and thus an initial flux of material. The convergence velocity can then be calculated and used to calculate the new geometry of the aggregate for a specific time step. For each time step, the porosity, contact area and convergence velocity are updated. The changes in porosity and contact area are evaluated for the various hold durations. The model results may be converted into a strength gain with time if we assume that strengthening is directly proportional to the increase in contact area: the quantity of the contact. Thus $\Delta\mu_x \sim (1 - A_c/A_{c0})$, where A_c is the final contact area and A_{c0} is the initial contact area. Model results for

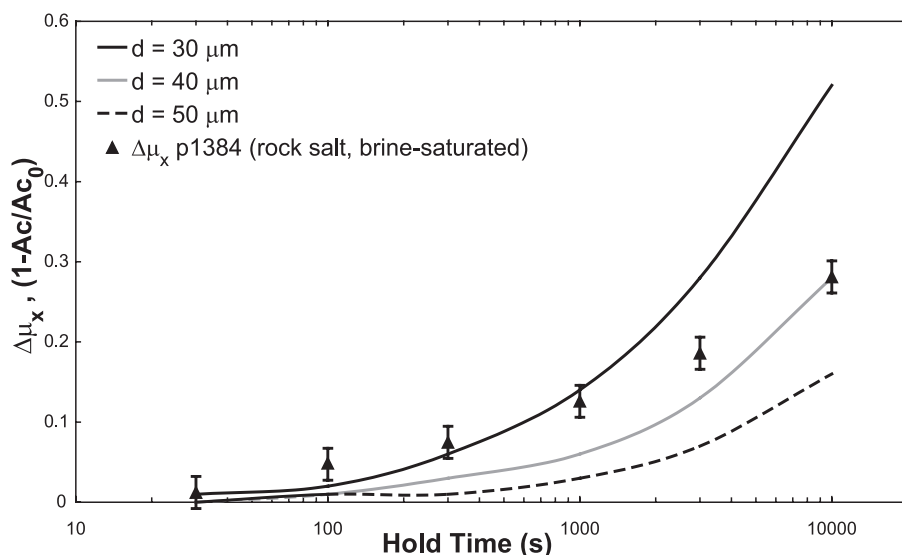


Figure 11. Plot showing model predictions for restrengthening (increase in contact area) by compaction via pressure solution using different values for the grain size. Also shown are the experimental data from experiment p1384 (rock salt, brine-saturated).

different grain sizes are compared to the experimental data in Figure 11. For comparison, we also show the results for the short hold periods. From Figure 11, it is clear that an increase in contact area via pressure-solution-aided compaction cannot explain the strengthening observed at short hold periods. Conversely, most of the strengthening at longer hold periods fits reasonably well with the model predictions. Discrepancies between the model predictions and the experimental results potentially are related to uncertainties in the measured porosities, instantaneous grain size and to the fact that the model is a gross oversimplification of the actual geometry of the gouges, i.e., it is based on the assumption that all grains are spherical, are of uniform size, and are packed as a simple cubic array. Despite this, the model results provide additional support for our interpretation of the physical-chemical processes responsible for the restrengthening at different timescales. For hold periods smaller than ~ 1000 s, no significant restrengthening is predicted. Moreover, the model shows that we have to take the current state of the gouge at the start of the hold period into account, since using different starting porosities (and grain sizes) yields different results.

5.2. Implications for Strength Recovery in Natural Faults Under Hydrothermal Conditions

[25] In the previous sections, we have shown that strengthening of fault gouges under conditions where pressure solution is active is essentially a combination of intrinsic strengthening of the sliding contacts (Dieterich-type healing), a reduction in porosity requiring dilational work to be done upon resliding, and an increase in contact area by compaction via pressure solution. Previous studies have primarily focused on Dieterich-type healing and have shown that this process is log linearly dependent on the hold time. Conversely, compaction via pressure solution is not log linearly dependent on the hold time and is a strong function of the instantaneous porosity and grain size.

Although seismic estimates of fault healing appear to be consistent with Dieterich-type healing relations from the laboratory [e.g., *Marone*, 1998a], the rates and magnitude of strength recovery in natural fault gouges under hydrothermal conditions may be significantly underestimated. A quantitative understanding of healing rates in natural fault gouges must account for the operation of pressure solution and therefore requires a detailed knowledge of the “state” of the gouge (i.e., the porosity and grain size). With some exceptions [*Bos and Spiers*, 2000, 2002a; *Niemeijer and Spiers*, 2006, 2007; *Sleep*, 1995, 1997], previous models for healing aided by pressure solution have largely neglected the effect of instantaneous porosity. Moreover, we have shown that the presence of a phyllosilicate phase significantly lowers the healing rate owing to the lower porosity attained during steady state sliding. Also, the presence or absence of a throughgoing foliation formed by the phyllosilicate phase might significantly affect the healing rates [*Niemeijer and Spiers*, 2006]. Therefore, care must be taken when using microphysical models of compaction via pressure solution to predict healing rates and recurrence times for natural fault gouges under hydrothermal conditions.

6. Conclusions

[26] A number of slide-hold-slide experiments were performed on simulated fault gouges of salt and salt-muscovite mixtures in the presence of brine. These experiments were designed to investigate the effect of pressure solution, and other mechanisms, on the healing behavior of fault gouges. It is apparent from these experiments that:

[27] 1. The healing rates in fault gouges consisting of salt in the presence of brine are high (friction increases by up to 0.285 per decade) and are two times higher than those in fault gouges consisting of salt-muscovite mixtures (up to 0.14 per decade).

[28] 2. Healing in our experiments was found to be a combination of three processes: (1) contact strengthening

(Dieterich-type healing); (2) reduction in porosity, requiring work against the normal stress upon reshear; and (3) increased contact area associated with compaction via pressure solution.

[29] 3. A microphysical model for compaction via pressure solution is capable of reproducing the effects of contact growth and extension at intermediate and longer hold durations (>1000 s), and implies that grain-boundary welding is responsible for healing at periods shorter than this.

[30] 4. In order to predict the magnitude and rates of healing in natural fault gouges under hydrothermal conditions, knowledge of the “state” (porosity, grain size and the presence of clay/phylosilicate particles) of the fault gouge is required.

[31] In conclusion, we have demonstrated that strength gain of fault gouges aided by pressure solution processes is a combination of dilational work done against the normal stress, an intrinsic strengthening of actively sliding contacts by pore reduction and grain interpenetration and an increase in contact area by compaction via pressure solution. In order to predict strength gain of natural fault gouges under conditions where pressure solution is operative, all three processes have to be taken into account and the composition, porosity and grain size (distribution) of the fault gouges have to be known.

[32] **Acknowledgments.** This work was supported by U.S. National Science Foundation grant EAR-0510182 and by NWO (Dutch Science Organisation) grant 825.06.003. This support is gratefully acknowledged. We also thank Chris Spiers and Stephen Cox for their constructive reviews, which helped improve this paper.

References

- Bjørkum, P. A. (1996), How important is pressure in causing dissolution of quartz in sandstones, *J. Sediment. Res.*, 66(1), 147–154.
- Bos, B., and C. J. Spiers (2000), Effect of phyllosilicates on fluid-assisted healing of gouge-bearing faults, *Earth Planet. Sci. Lett.*, 184, 199–210.
- Bos, B., and C. J. Spiers (2001), Experimental investigation into the microstructural and mechanical evolution of phyllosilicate-bearing fault rock under conditions favouring pressure solution, *J. Struct. Geol.*, 23(8), 1187–2002.
- Bos, B., and C. J. Spiers (2002a), Fluid-assisted healing processes in gouge-bearing faults: Insights from experiments on a rock analogue system, *Pure Appl. Geophys.*, 159, 2537–2566.
- Bos, B., and C. J. Spiers (2002b), Frictional-viscous flow of phyllosilicate-bearing fault rock: Microphysical model and implications for crustal strength profiles, *J. Geophys. Res.*, 107(B2), 2028, doi:10.1029/2001JB000301.
- Chester, F. M., and N. G. Higgs (1992), Multimechanism friction constitutive model for ultrafine quartz gouge at hypocentral conditions, *J. Geophys. Res.*, 97, 1859–1870.
- Dewers, T., and P. Ortoleva (1990), A coupled reaction/transport/mechanical model for intergranular pressure solution, stylolites, and differential compaction and cementation in clean sandstones, *Geochim. Cosmochim. Acta*, 54, 1609–1625.
- Dysthe, D. K., F. Renard, F. Porcheron, and B. Rousseau (2002), Fluid in mineral interfaces—molecular simulations of structure and diffusion, *Geophys. Res. Lett.*, 29(7), 1109, doi:10.1029/2001GL013208.
- Fredrich, J. T., and B. Evans (1992), Strength recovery along simulated faults by solution transfer processes, in *Rock Mechanics: Proceedings of the 33rd U.S. Symposium*, edited by J. R. Tillerson and W. Wawersik, pp. 121–130, A. A. Balkema, Brookfield, Vt.
- Frye, K. M., and C. Marone (2002), Effect of humidity on granular friction at room temperature, *J. Geophys. Res.*, 107(B11), 2309, doi:10.1029/2001JB000654.
- Gundersen, E., D. K. Dysthe, F. Renard, K. Bjørlykke, and B. Jamtveit (2002), Numerical modelling of pressure solution in sandstone, rate-limiting processes and the effect of clays, in *Deformation Mechanisms, Rheology and Tectonics*, edited by S. De Meer, et al., pp. 41–60, Geol. Soc., London.
- He, W., A. Hajash, and D. Sparks (2002), A model for porosity evolution during creep compaction of sandstones, *Earth Planet. Sci. Lett.*, 197, 237–244.
- Heald, M. T. (1959), Significance of stylolites in permeable sandstones, *J. Sediment. Petrol.*, 29, 251–253.
- Hickman, S., R. Sibson, and R. Bruhn (1995), Introduction to special section: Mechanical involvement of fluids in faulting, *J. Geophys. Res.*, 100, 12,831–12,840.
- Kanagawa, K., S. F. Cox, and S. Zhang (2000), Effects of dissolution-precipitation processes on the strength and mechanical behavior of quartz gouge at high-temperature hydrothermal conditions, *J. Geophys. Res.*, 105, 11,115–11,126.
- Karner, S. L., C. Marone, and B. Evans (1997), Laboratory study of fault healing and lithification in simulated fault gouge under hydrothermal conditions, *Tectonophysics*, 277, 41–55.
- Kirby, S. H., and C. H. Scholz (1984), Chemical effects of water on the strength and deformation of crustal rocks, *J. Geophys. Res.*, 89, 4611.
- Lehner, F. K. (1995), A model for intergranular pressure solution in open systems, *Tectonophysics*, 245, 153–170.
- Marone, C. (1998a), The effect of loading rate on static friction and the rate of fault healing during the earthquake cycle, *Nature*, 391, 69–71.
- Marone, C. (1998b), Laboratory-derived friction laws and their application to seismic faulting, *Annu. Rev. Earth Planet. Sci. Lett.*, 26, 643–696.
- Nakatani, M., and C. H. Scholz (2004), Frictional healing of quartz gouge under hydrothermal conditions: 1. Experimental evidence for solution transfer healing mechanism, *J. Geophys. Res.*, 109, B07201, doi:10.1029/2001JB001522.
- Niemeijer, A. R., and C. J. Spiers (2002), Compaction creep of quartz-muscovite mixtures at 500°C: Preliminary results on the influence of muscovite on pressure solution, in *Deformation Mechanisms, Rheology and Tectonics*, edited by S. De Meer, et al., pp. 61–72, Geol. Soc., London.
- Niemeijer, A. R., and C. J. Spiers (2005), Influence of phyllosilicates on fault strength in the brittle-ductile transition: Insights from rock analogue experiments, in *High-Strain Zones: Structure and Physical Properties*, edited by D. Bruhn and L. Burlini, pp. 303–327, Geol. Soc., London.
- Niemeijer, A. R., and C. J. Spiers (2006), Velocity dependence of strength and healing behavior in simulated phyllosilicate-bearing fault gouge, *Tectonophysics*, 427, 231–253.
- Niemeijer, A. R., and C. J. Spiers (2007), A microphysical model for strong velocity weakening in phyllosilicate-bearing fault gouges, *J. Geophys. Res.*, 112, B10405, doi:10.1029/2007JB005008.
- Niemeijer, A. R., C. J. Spiers, and B. Bos (2002), Compaction creep of quartz sand at 400–600°C: Experimental evidence for dissolution-controlled pressure solution, *Earth Planet. Sci. Lett.*, 195, 261–275.
- Paterson, M. S. (1995), A theory for granular flow accommodated by material transfer via an intergranular fluid, *Tectonophysics*, 245, 135–151.
- Renard, F., P. Ortoleva, and J.-P. Gratier (1997), Pressure solution in sandstones: Influence of clays and dependence on temperature and stress, *Tectonophysics*, 280, 257–266.
- Renard, F., A. Park, P. Ortoleva, and J.-P. Gratier (1999), An integrated model for transitional pressure solution in sandstones, *Tectonophysics*, 312, 97–115.
- Renard, F., D. Dysthe, J. Feder, K. Bjørlykke, and B. Jamtveit (2001), Enhanced pressure solution creep rates induced by clay particles: Experimental evidence in salt aggregates, *Geophys. Res. Lett.*, 28, 1295–1298.
- Scholz, C. H. (2002), *The Mechanics of Earthquakes and Faulting*, 471 pp., Cambridge Univ. Press, New York.
- Schutjens, P. M. T. M., and C. J. Spiers (1999), Intergranular pressure solution in NaCl: Grain-to-grain contact experiments under the optical microscope, *Oil Gas Sci. Technol.*, 54, 729–750.
- Scott, D. R., C. J. Marone, and C. G. Sammis (1994), The apparent friction of granular fault gouge in sheared layers, *J. Geophys. Res.*, 99, 7231–7246.
- Sleep, N. H. (1995), Ductile creep, compaction, and rate and state dependent friction within major fault zones, *J. Geophys. Res.*, 100, 13,065–13,080.
- Sleep, N. H. (1997), Application of a unified rate and state friction theory to the mechanics of fault zones with strain localization, *J. Geophys. Res.*, 102, 2875–2895.
- Spiers, C. J., P. M. T. M. Schutjens, R. H. Brzesowsky, C. J. Peach, J. L. Liezenberg, and H. J. Zwart (1990), Experimental determination of constitutive parameters governing creep of rocksalt by pressure solution, in *Deformation Mechanisms, Rheology and Tectonics*, edited by S. De Meer et al., pp. 215–227, Geol. Soc., London.
- Spiers, C. J., S. De Meer, A. R. Niemeijer, and X. Zhang (2004), Kinetics of rock deformation by pressure solution and the role of thin aqueous films,

- in *Physicochemistry of Water in Geological and Biological Systems*, edited by S. Nakashima et al., pp. 129–158, Univ. Acad. Press, Tokyo.
- Tenthorey, E., and S. F. Cox (2006), Cohesive strengthening of fault zones during the interseismic period: An experimental study, *J. Geophys. Res.*, *111*, B09202, doi:10.1029/2005JB004122.
- Tenthorey, E., S. F. Cox, and H. F. Todd (2003), Evolution of strength recovery and permeability during fluid-rock reaction in experimental fault zones, *Earth Planet. Sci. Lett.*, *206*, 161–172.
- Yasuhara, H., C. Marone, and D. Elsworth (2005), Fault zone restrengthening and frictional healing: The role of pressure solution, *J. Geophys. Res.*, *110*, B06310, doi:10.1029/2004JB003327.
-
- D. Elsworth and A. Niemeijer, Department of Energy and Mineral Engineering, Pennsylvania State University, 230A Hosler Building, University Park, PA 16802, USA. (arn3@psu.edu)
- C. Marone, Department of Geosciences, Pennsylvania State University, University Park, PA 16802, USA.